J Mater Sci (2012) 47:241–250
DOI 10.1007/s10853-011-5791-2

Relevance of instrumented nano-indentation for the assessment of the mechanical properties of eutectic crystals and α-Al grain in cast aluminum alloys

Mitsuhiro Okayasu · Satoshi Takasu · Mamoru Mizuno

Received: 9 May 2011 / Accepted: 12 July 2011 / Published online: 27 July 2011

Abstract To better understand the material properties of cast aluminum alloys, the mechanical properties of microscopic structures (the eutectic structure and the α-Al phase) have been systematically examined using a special nano-indentation hardness test machine. In this approach, a triangular indentation is applied directly to the eutectic structure or α-Al phase, and the mechanical properties evaluated through hardness and load-strain relationships. The hardness of the eutectic phase varied, depending on the structural characteristics of the different intermetallic compounds. High values of hardness were obtained structures of the DO_3 type, e.g., Al_5FeSi, but low hardness for $CuAl_2$ and Mg_2Si. The hardness of $CuAl_2$ and Mg_2Si had almost the same values as that of the α-Al matrix. In addition, from the nano-indentation hardness test, the effects of α-Al grain characteristics on the mechanical properties were clarified. The hardness of the α-Al grain was linearly related to the grain size and the distance from the grain boundary, where the higher the hardness, the smaller the grain size and the closer to the grain boundary. The hardness level was attributed to the different severity of slip resistance of the atoms during the indentation loading.

Introduction

Casting technologies (gravity casting and pressure casting) are widely utilized in manufacturing processes for producing various engineering components. The advantages of casting are high productivity and the possibility to produce components with complicated geometries [1]. In recent years, light weight materials, e.g., aluminum and magnesium, have received special attention for many engineering applications, because of the issues of gas emissions and global warming. The use of cast aluminum alloys has increased, particularly for automotive and electrical parts. Aluminum–silicon alloys are widely used in different field of industry due to their high fluidity. Other advantages are high resistance to corrosion and a reduction in the shrinkage rate. With the addition of copper to cast Al–Si alloys, the mechanical properties, e.g., material hardening and tensile strength, are significantly improved. The disadvantages of Al–Si–Cu alloys are low castability and low corrosion resistance. Commercial Al–Si–Cu alloys have been available for many years. The compositions lie mostly within the ranges 3–11% Si and 1–10% Cu, although higher proportions of silicon (around 10%) are used in Al–Si–Cu alloys for high pressure diecastings [2]. A number of aluminum diecast components have been recently used for various automotive parts, e.g., cylinder blocks and transmission cases. Magnesium is also a significant element for the creation of cast aluminum alloys with high corrosion resistance, good machinability, and attractive appearance. The magnesium content of the binary alloys ranges from 4 to 10%. There are some issues in Al–Mg alloys, namely low castability and severer oxidation, when large amounts of magnesium are added in the molten state.

There are various eutectic structures (Si, Al_2Cu, Al_4FeSi, Mg_2Si, and Al_3Mg_2) formed in cast aluminum alloys. The material characteristics of each microscopic structure affect the mechanical properties of the Al alloys. One of the authors has investigated the effects of Si content on the tensile properties of cast aluminum alloys, using several

M. Okayasu (✉) · S. Takasu · M. Mizuno
Department of Machine Intelligence and Systems Engineering, Akita Prefectural University, 84-4 Aza Ebinokuchi, Tsuchiya, Yurihonjo, Akita 015-0055, Japan
e-mail: okayasu@akita-pu.ac.jp

Table 1 Chemical compositions of the cast aluminum alloys

	Cu	Si	Mg	Fe	Ni	Al	σ_{UTS} (MPa)	ε_f (%)
AC2A	4.6	5.0	<0.25	<0.8	<0.3	Bal.	180	2
AC7A	<0.1	<0.2	4.0	<0.1	<0.05	Bal.	210	12
AC8A	1.0	12.0	1.0	<0.8	11.5	Bal.	170	2.5
ADC1	<1.0	12.0	<0.3	<1.3	<0.5	Bal.	298	3.5
ADC6	<0.1	<1.0	3.3	<0.8	<0.1	Bal.	309	5
ADC12	2.5	10.8	<0.3	<1.3	<0.5	Bal.	329	2.5

alloys, with different amounts of Si. It appeared that the tensile strength and ductility decrease significantly with increasing proportion of silicon [3]. The addition of silicon to Al–Mg alloys can promote the precipitation of Mg_2Si and $\beta(Al_3Mg_2)$, and these phases can lead to deleterious effects on their ductility and toughness [4]. Yoo et al. [5] have investigated the hardness of Mg_2Si using a micro-Vickers hardness tester, and shown that the hardness level in Mg_2Si is much higher than that in the matrix. The mechanical properties of aluminum–copper cast alloys rely on a combination of precipitation hardening together with dispersion hardening. The maximum strengthening of Al–Cu alloy is created by adding between 4 and 6% copper (Al–4.7Cu–0.7Ag–0.3 Mg) although it also depends on the influence of other constituents present. The cast Al–Cu alloy mainly consists of the α-Al matrix and θ-$CuAl_2$ eutectic structures. The α-phase has a high ductility whereas the θ-phase is brittle [6]. The microstructure of Al–Si–Cu alloys is formed by multicomponent eutectic reactions, e.g., $L \rightarrow Al + CuAl_2 + \beta(Al_5FeSi) + Si$ [7, 8]. Iron is one of the critical alloying elements (impurity elements) in cast aluminum alloys. In the solidification process, several iron-based intermetallic compounds are created, such as Al_3Fe, α(Al–Fe–Si) and β(Al–Fe–Si). These compounds are considered to have high hardness and brittleness, resulting in deleterious effects on the mechanical properties of the Al alloys. Although there are several eutectic structures, the material properties of eutectic systems have not been examined in detail.

Some researchers have investigated the relationship between the size of the α-Al grains and their tensile properties using the Hall–Petch equations [9]. Osório et al. [10] have studied the effect of secondary dendrite arm spacing (DASII), on the tensile properties of Al–9%Si alloy, where the ultimate tensile strength and elongation increase with decreasing DASII. Kanazawa and Okayasu have also examined the effects of grain size on the tensile properties of cast Al–Si–Cu alloy, and it appeared that there are Hall–Petch equations between the DASII and the observed 0.2% proof stress [11]. Another approach was carried out by Iwahori et al. [12] in which the tensile strength of the interface between the abnormal and normal microstructure for Al–Si–Cu alloys was examined. One of their conclusions was that the interface strength is as low as 88.2 MPa, which is much lower than that for the normal structure. Several experiments have been carried out to examine the mechanical properties of cast aluminum alloys, but the material properties in specific microscopic areas, e.g., α-Al phase, have not been properly investigated.

Even though the information concerning the microscopic characteristics of the eutectic structure and α-Al phase might not always be required, these can sometimes be significant and may permit accurate and clear descriptions of the material properties of the cast aluminum alloys. This is because the eutectic structure and α-Al phase are formed with different size structures and various morphologies. Furthermore, these phases are variably distributed. The purpose of this study was therefore to explore the

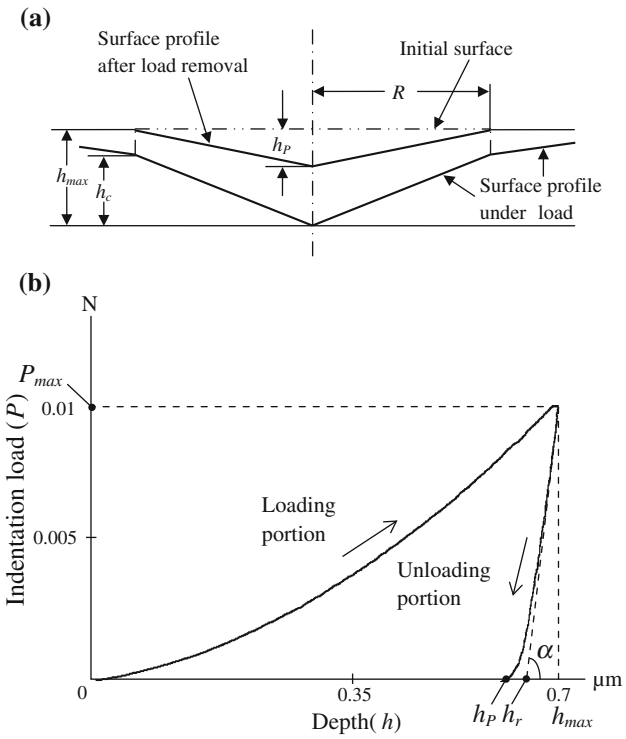

Fig. 1 **a** Schematic illustration of the indentation process. **b** Typical load-depth curve from a nano-indentation test

mechanical properties of microscopic areas of cast Al alloys using a nano-indentation hardness test machine.

Experimental

Materials and experimental procedures

Six cast aluminum alloys were selected for the present investigation, (i) AC2A, (ii) AC7A, (iii) AC8A, (iv) ADCl, (v) ADC6, and (vi) ADC12, as specified in the Japan Indusstrial Standard (JIS). Those Al alloys are representative cast aluminum alloys, widely employed for mechanical and electrical parts. Their chemical composition and tensile properties are summarized in Table 1. The cast samples were produced in atmosphere by conventional gravity casting and high pressure diecasting. The gravity cast samples were created using a mould: 600 × 90 × 40 mm^3. The temperatures of the molten metals for the gravity casting process were more than 973 K. For the high pressure diecasting process, the molten metal was injected into the die cavity via the shot sleeve after being poured by a ladle; this is the cold chamber diecasting system. The injection speeds at the gate were 40 m/s. The shape of the die cavity was a rectangle 40 × 20 × 5 mm^3. The other diecasting conditions were as follows: the temperature of the molten metal in crucible was 973 K, the die temperature in the cavity near the gate was approximately 473 K and the shot time lag was less than 0.5 s.

The microstructural observations of all cast samples were conducted using a scanning electron microscope (SEM, S-4300 Hitachi) and an energy dispersive X-ray spectrometer (EDX, EMAX-7000 Horiba). Both SEM and EDX observations were carried out at 15 kV.

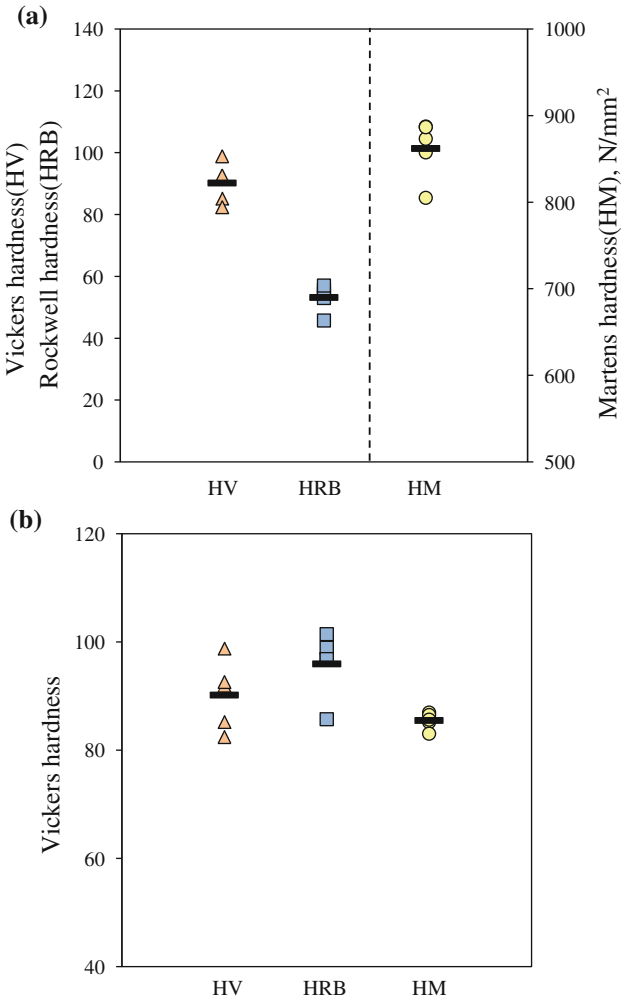

Fig. 3 Hardness of the gravity cast ADC12 sample obtained using several hardness testers (*HV* micro-Vickers hardness, *HRB* Rockwell hardness, and *HM* ultra-micro-hardness)

Martens hardness (HM)

The material hardness was measured using a dynamic ultra-micro-hardness tester (DUH-211 Shimadzu). The advantage of this hardness system is that the hardness in tiny areas (nano-size) can be examined. The minimum indentation load of this hardness tester is 0.1 mN. With this test system, the Martens hardness (HM) is obtained, defined as the maximum applied load, P_{max}, divided by contact area A:

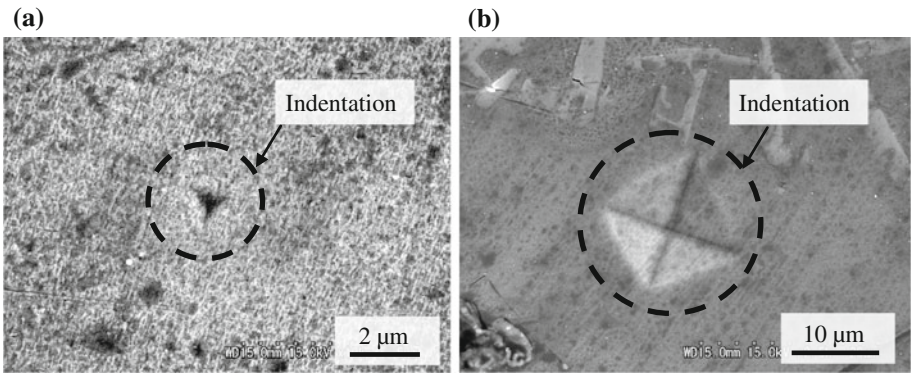

Fig. 2 SEM micrographs showing the indentation obtained by **a** ultra-micro-hardness test and **b** micro-Vickers hardness test

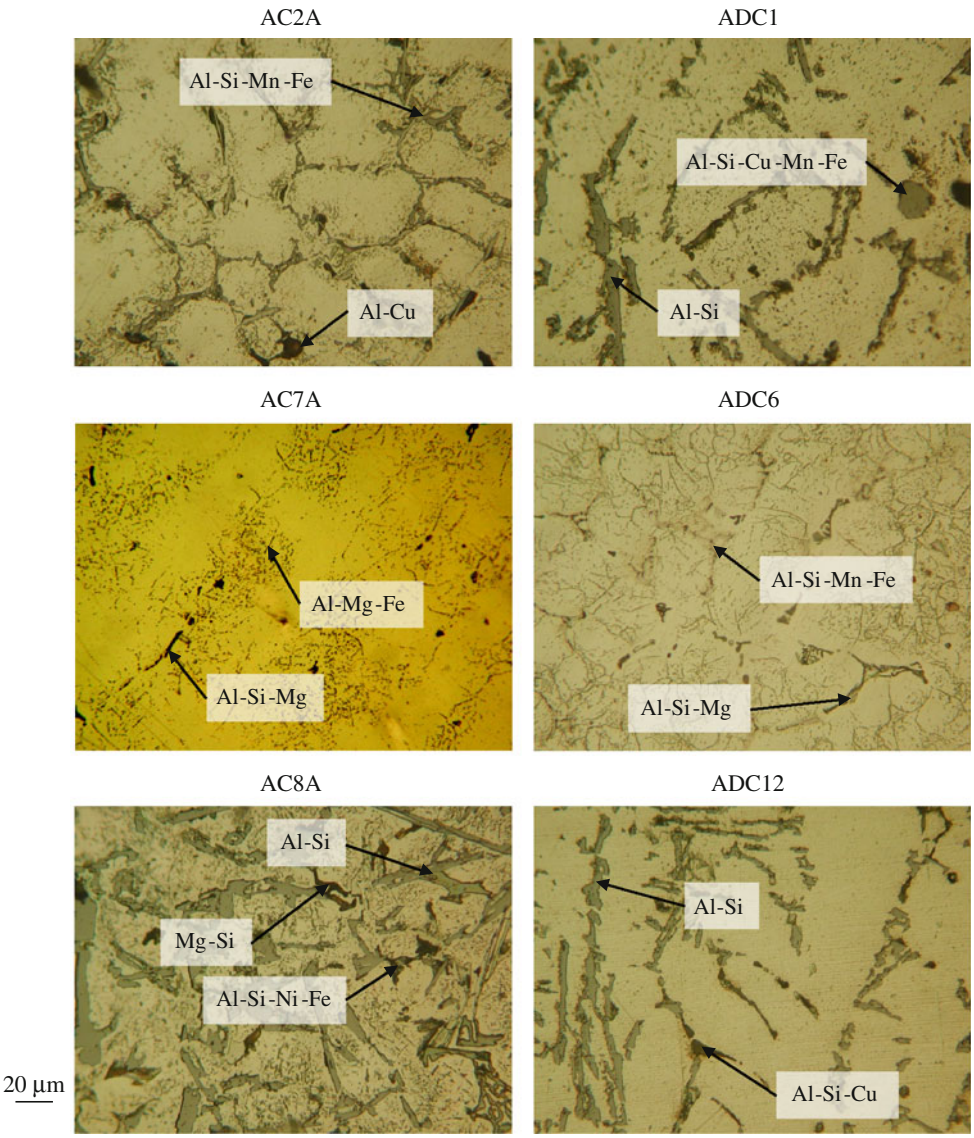

Fig. 4 Optical micrographs of various gravity cast samples

$$\mathrm{HM} = \frac{P_{\max}}{A(h)} \approx \frac{P_{\max}}{26.43h^2} \tag{1}$$

$$\text{with } A(h) = \frac{3\sqrt{3}\tan(a)}{\cos(a)}h^2 \tag{1a}$$

where h is the penetration depth, and the parameter a refers to the face angle of the indenter, which is, 115°. Figure 1a, b give a schematic representation of the indentation process and typical indentation load versus depth curve, respectively. In this case, R is the radius of the contact circle defined by the indenter, h_p is the plastic depth, h_c is the contact depth (see Fig. 1a), and h_r is the depth obtained at the intercept of the linear unload versus depth portion with the x-axis (Fig. 1b).

In this study, the microhardness of the microscopic structure was examined using a triangle indentation with several indentation load conditions (1, 10, and 20 mN). For the hardness measurement, the sample surface was polished to a mirror finish using colloidal silica. Figure 2a, b display the SEM micrographs for the α-Al phase of gravity cast ADC12 showing the ultra-micro-hardness indentation (HM) and traditional micro-Vickers hardness indentation (HV), respectively. The marks for MH and HV were obtained from the indentation loads at $P_{\max} = 1$ and 100 mN, respectively. Note that the indentation load of 100 mN is the minimum available load for HV but 1 mN is not the minimum for HM. Figure 2 shows clearly the different indentation sizes, where a large indentation, over 14.1 μm in diameter is for the HV, a value more than ten times greater than that for the HM. We are convinced from Fig. 2 that the ultra-micro-hardness test machine can be used to measure hardness in a tiny area.

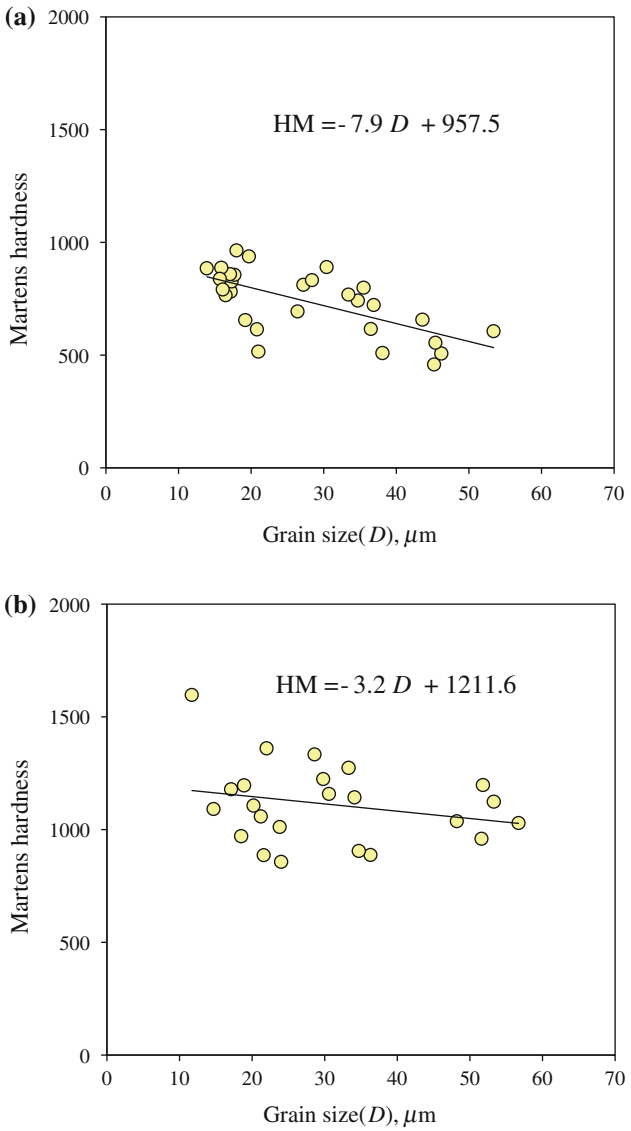

Fig. 5 Relationship between hardness and grain size for **a** diecast sample and **b** gravity sample (ADC12)

Figure 3 shows the hardness of the cast sample ADC12 as measured by three different testing machines (Rockwell (HRB)-, micro-Vickers-, and ultra-micro-hardness). In this case, the hardness measurement for HM was executed with low indentation load (P_{max} = 10 mN) to examine the hardness in the middle of the α-Al phase. On the other hand, the hardness of several α-grains together with eutectic structures were measured by the HRB and HV testers. The hardness shown in Fig. 3a are identified as Vickers hardness (HV), Rockwell hardness B scale (HRB), and Martens hardness (HM). Figure 3b shows the hardness data for HRB and HM from Fig. 3a converted to Vickers hardness (HV) in order to compare the data. In this case, general hardness conversion chart was employed [13]. It is clear from Fig. 3b that the hardness levels examined by the Rockwell and micro-Vickers are high compared to the ultra-micro-hardness measurements. This is due to the incorporation of hardness measurements of hard eutectic structures in addition to the α-Al phases for HRB and HV whereas only the soft α-Al phases are measured for HM.

In this case, the Vickers hardness was estimated from HM as follows [14]:

$$\mathrm{HV} = 0.0924 \times H_{\mathrm{IT}} \tag{2}$$

$$\text{with } H_{\mathrm{IT}} = \frac{P_{\max}}{A_p} \tag{2a}$$

$$A_p = 23.96 \times h_c^2 \quad \text{for triangular pyramid indentation} \tag{2b}$$

$$A_p = 24.50 \times h_c^2 \quad \text{for Vickers indentation} \tag{2c}$$

$$h_c = h_{\max} - \varepsilon(h_{\max} - h_r) \tag{2d}$$

where H_{IT} is the indentation hardness, N/mm^2. Because triangular pyramid indentation is used, $\varepsilon = 0.75$ [14]. Using the parameters shown in Fig. 1b, h_c can be determined using Eq. 2d to give $h_c = 0.7 \times 10^{-3}$ mm−0.75 (0.7–0.65 × 10^{-3} mm). In terms of Eqs. 2a and 2c, A_p and

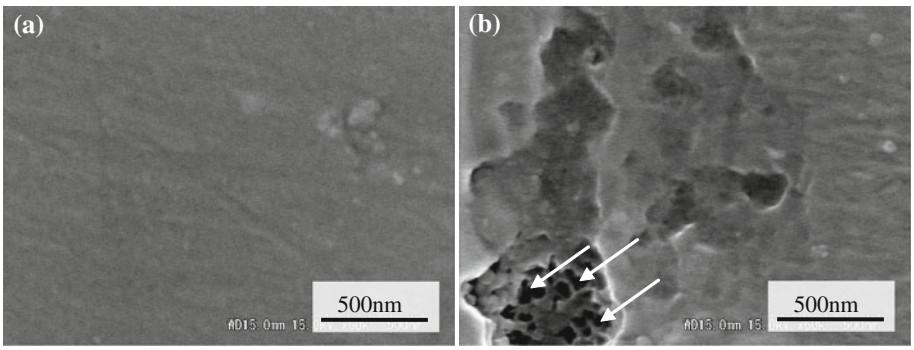

Fig. 6 SEM micrographs showing the microstructures for **a** gravity sample and **b** diecast sample

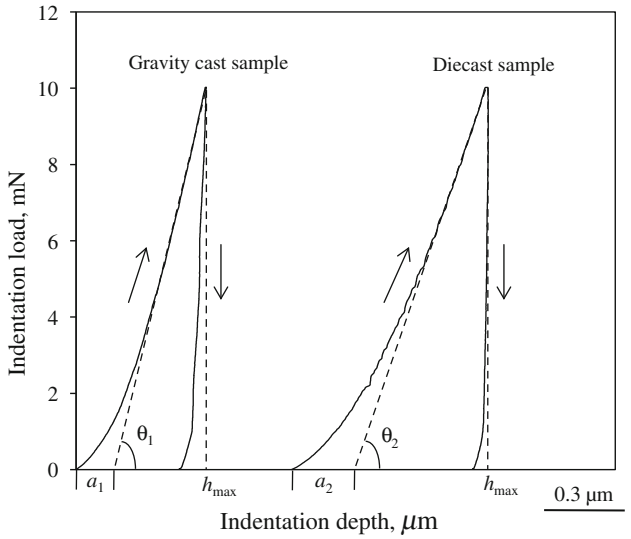

Fig. 7 Indentation load-depth curves for the gravity and diecast samples obtained at the center of the α-Al phase (ϕ20 μm)

H_{IT} are approximately $A_p = 23.96 \times 0.00066$ mm^2 and $H_{IT} = 0.01$ N/1.05×10^{-5} mm^2, respectively. Using the H_{IT} value, HV can be estimated to give HV $= 0.0924 \times 950.9 = 87.9$ N/mm^2.

Results and discussion

Mechanical properties of α-Al grains

Figure 4 shows the optical micrographs of the six aluminum alloys. The microstructures consist of regular α-Al phases and eutectic structures. As seen, various eutectic structures, formed with equiaxial and fibrous shapes, can be obtained depending on the aluminum alloys, e.g., (i) AC2A: Al–Si–Mn–Fe base and Al–Cu base, (ii) AC7A: Al–Mg–Fe and Al–Si–Mg, (iii) AC8A: Al–Si–Ni–Fe, Al–Si–Mg–Fe, Al–Si, and Mg–Si, (iv) ADC1: Al–Si and Al–Si–Cu–Mn–Fe, (v) ADC6: Al–Si-Mn–Fe and Al–Si-Mg, and (vi) ADC12: Al–Si–Cu, Al–Si–Fe, and Al–Si. The eutectic structures can be classified into several eutectic systems, Al–Si type, Mg–Si type, Al–Cu type, Al–*x*–Fe type and the other minor structures. Details of their material characteristics will be interpreted in a later section of this article.

Figure 5 shows the variation of HM hardness as a function of grain size (α-Al phase) for sample ADC12, made by both the diecasting and gravity processes. It should be noted first that the grain sizes were measured by the linear intercept method, and the hardness measurements were carried out in the center of each α-Al grain. As seen in Fig. 5, there is an almost linear relationship between the grain size and hardness for both samples although the data plots are relatively scattered for the gravity cast samples. In this case, the larger the grain size, the lower the hardness. The linear relationships obtained, approximated by the least squares method, are as follows:

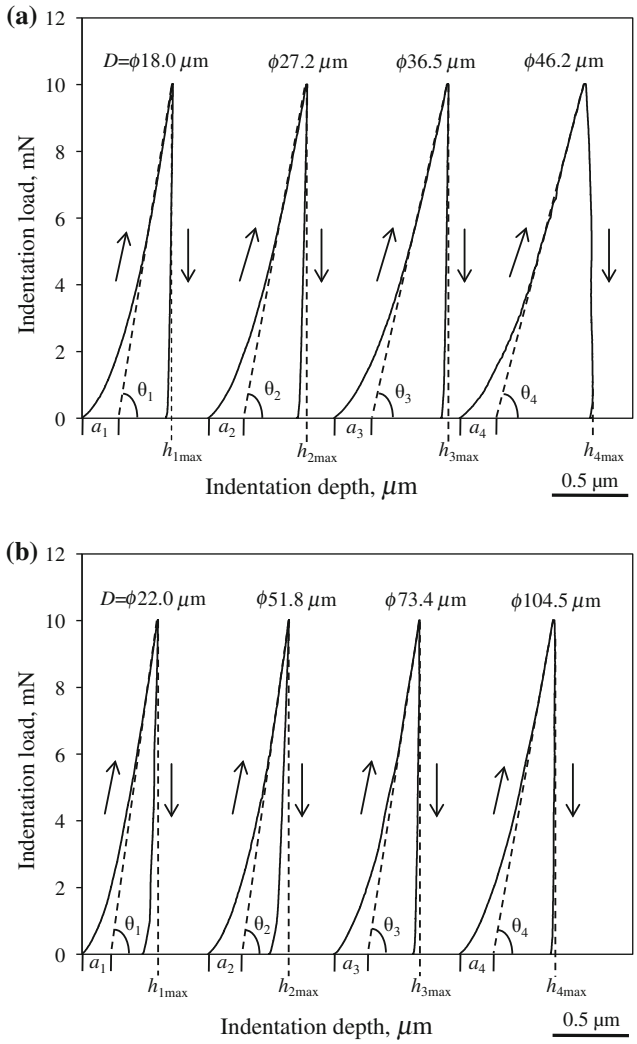

Fig. 8 Indentation load and indentation depth curves obtained for various grain sizes (D): **a** diecast sample and **b** gravity sample

$$\mathrm{HM} = -7.9\mathrm{D} + 957.5 \; (D = 10 \sim 60\,\mu\mathrm{m}) \text{ for diecasting} \tag{3a}$$

$$\mathrm{HM} = -3.2\mathrm{D} + 1211.6 \; (D = 10 \sim 60\,\mu\mathrm{m}) \text{ for gravity casting} \tag{3b}$$

where D is the grain size (μm). Note, in this case, both equations are applicable for the sample with the grain size between 10 and 60 μm. It is also seen in Fig. 5 that the hardness levels for the diecast samples are lower overall than those for the gravity ones. This might be due to the defects in the diecast samples, e.g., porosity [15]. It is generally considered that, in the diecast sample, a large degree of porosity is produced as a result of the high speed

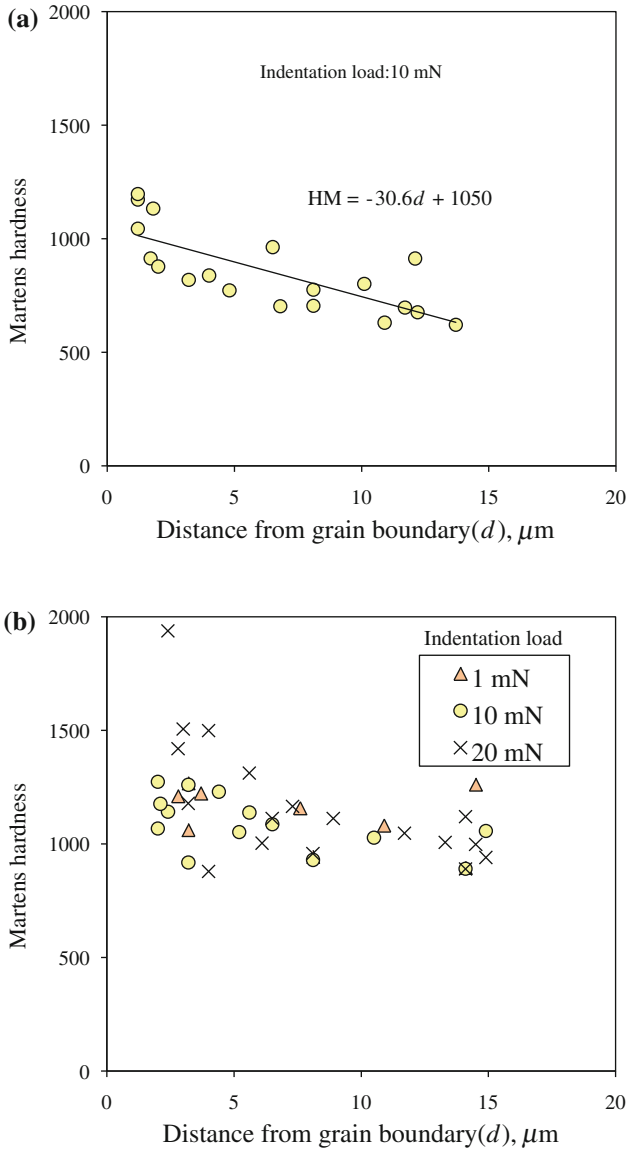

Fig. 9 Relationship between hardness and distance from grain boundary for **a** diecast sample and **b** gravity sample (ADC12)

and pressure injection system. To verify this, direct observation of the microstructure in both gravity and diecast samples was conducted. Before the observation, the sample surfaces were etched with an etchant: 75 mL (H_2O) and 25 mL (65%HNO_3), for 120 s. Figure 6 displays the SEM images of both microstructures observed at high magnification, ×60,000. It is clear from Fig. 6 that the surface roughness is apparently different, e.g., smooth surface in the gravity sample, and rough face in the diecast one. It is interest to mention that the rough surface for the diecast sample consists of the small tiny holes about 100 nm in diameter, as indicated by the arrows. Those may be arising from the porosity or dislocation core although further study will be required.

It is also considered from Fig. 5 that the linear relationship between grain size and mechanical properties is described by the Hall–Petch relationships. In previous work, the Hall–Petch equations were applied to cast aluminum alloys using their tensile test data, e.g., DASII vs. $\sigma_{0.2}$ [10, 11]. Since there are various complicating factors in the microstructure (different α grain size, different α grain morphologies, and various eutectic structures), as mentioned previously, our approach, which only considers the mechanical properties of each α-Al grain, leads to more appropriate Hall–Petch relationships.

Figure 7 shows the representative indentation load versus indentation depth curves for samples ADC12. These were obtained form the α-Al phase with almost same grain size about ϕ20 μm. Based upon the load-depth relationships, the material properties (strength and ductility) can be clarified. It is clear from both load-depth relationships, the slope of the linear loading portion (θ) and the maximum depth (h_{max}) are different, since lower θ and greater h_{max} are obtained for the diecast sample. The θ and h_{max} values for the diecast sample are about 12% lower and 50% higher than for the gravity cast sample.

Figure 8 displays the indentation load versus depth curves obtained for different grain sizes. It is clear that the slope of linear loading portion (θ) and the maximum depth (h_{max}) vary, with the higher slope and smaller depth obtained in small grains. Also confirmed is the important fact that the loading portion of the load versus depth can be divided into two different regions, the initial stage (nonlinear region), and the later stage (linear region), where the trend of the initial stage (a_n) is observed for all grains. The reason for this may be that during the indentation loading, the α-Al matrix is severely deformed because of the applied load, with a high stress concentration arising from the sharp edges of the triangle indentation.

To understand further the characteristic mechanical properties of the α-Al phase, the micro-hardness measurements were conducted for each α-phase including changing the measurement point on a diametrical direction from the grain boundary (GB). Figure 9 shows the variation of the HM hardness as a function of the distance from the GB for the ADC12 diecast and gravity samples. In this approach, three different indentation loads were used for the gravity sample measurements (1, 10, and 20 mN) but only one loading condition (10 mN) for the diecast samples. As can be seen, there are almost linear relationships for all conditions, even though a different slope is detected for the gravity samples, e.g., the higher the slope, the greater the load level. The linear relationships can be expressed as follows:

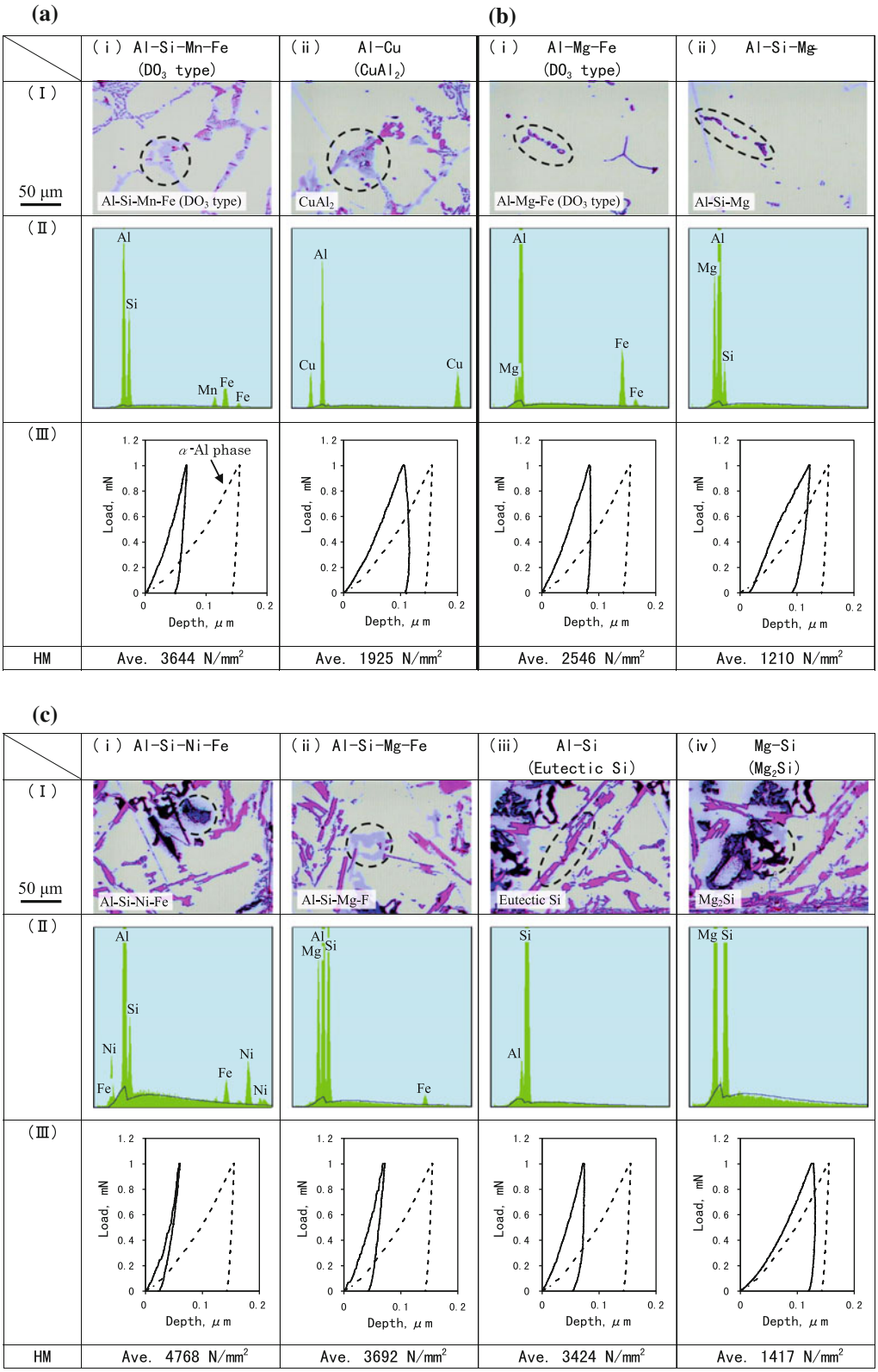

Fig. 10 Characterization of the eutectic structures in various cast Al alloys: **a** AC2A, **b** AC7A, **c** AC8A, **d** ADC1, **e** ADC6, and **f** ADC12. The dashed line (load versus depth): α-Al phase

(d) **(e)**

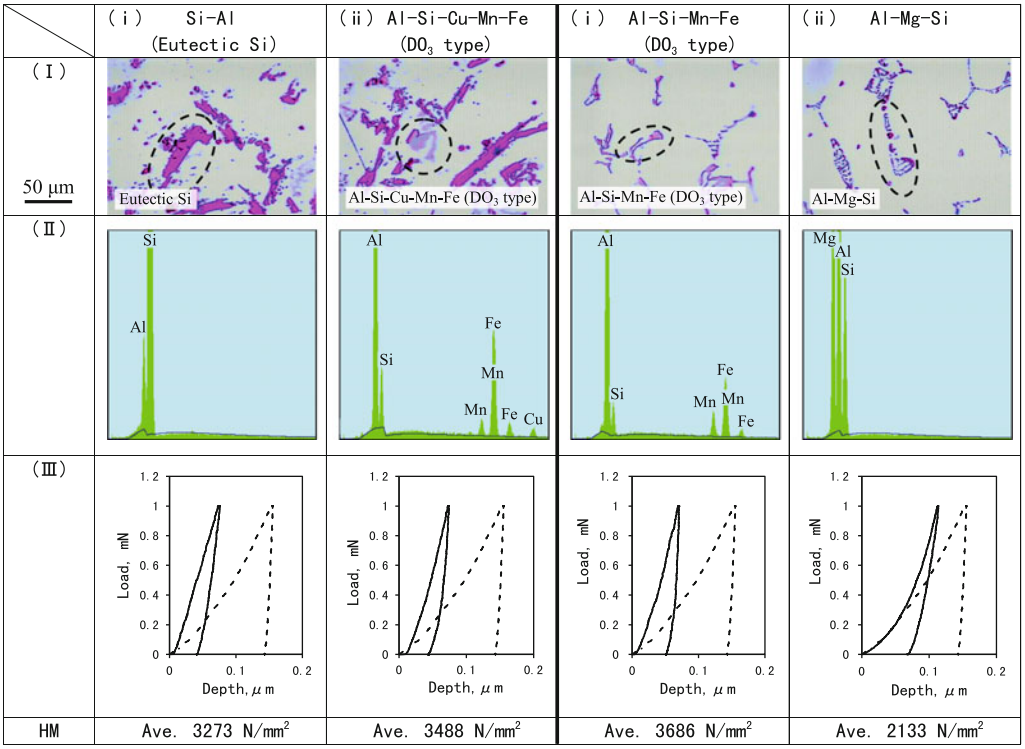

(f)

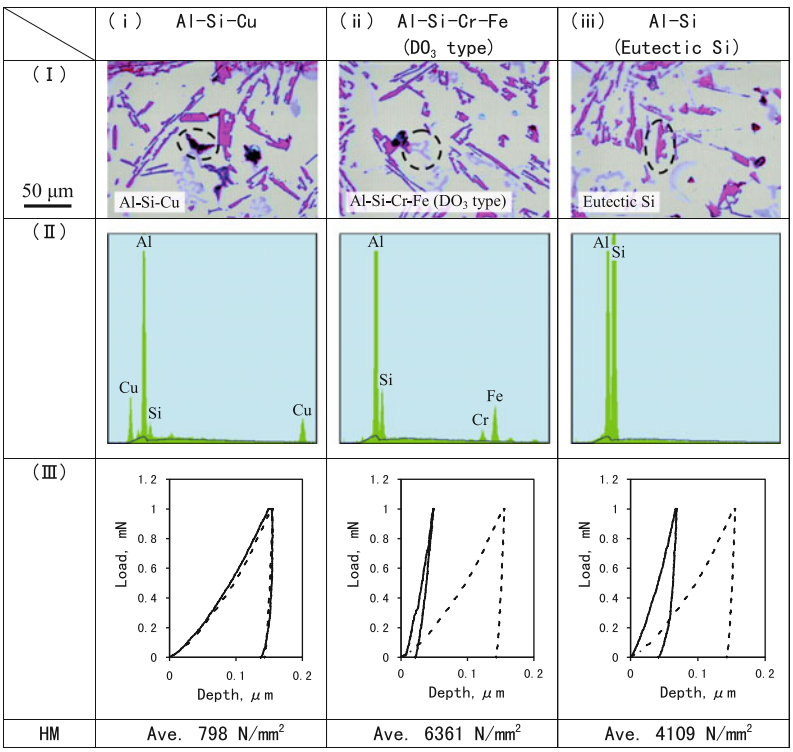

Fig. 10 continued

$$HM_{10\,mN} = -30.6d + 1050.0 \quad (d = \sim 15\mu m) \text{ for die casting} \tag{4a}$$

$$HM_{1mN} = -10.8d + 1204.1 \quad (d = \sim 15\mu m) \text{ for gravity casting} \tag{4b.1}$$

$$HM_{10\,mN} = -15.7d + 1183.4 \tag{4b.2}$$

$$HM_{20\,mN} = -37.8d + 1474.7 \tag{4b.3}$$

In this case, the different slopes might be caused by the different slip resistance of the atoms, where high slip resistance occurs when high indentation loading was executed in α-Al phase especially in areas adjacent to the grain boundaries.

Mechanical property of eutectic structures

The material hardness of the eutectic structures was investigated. In the aluminum alloys employed in this study, various eutectic structures were obtained, as described previously. Figure 10 summarizes the material properties of the eutectic structures, examined by SEM, EDX analysis and the nano-indentation hardness test. Note the load versus depth relations, which indicated by the dashed lines, are obtained in α-Al phase. It is interesting to mention that the hardness level varies significantly depending on the eutectic structure. From Fig. 10f, the hardness of the eutectic Si in ADC12 is 4109 N/mm^2 which is slightly lower than that of the Al–*x*–Fe-base structures (6361 N/mm^2), but obviously higher than that of the others, e.g. Al–Si–Cu (798 N/mm^2). Similar trends in the values of the eutectic hardness can be seen in the other materials. The high hardness of the Al–Si–*x*–Fe type is similar to the silicon nitride ceramics Si_3N_4 [16]. Such a high hardness would be influenced by the crystal structure of the intermetallic compound, i.e., DO_3 type. In contrast, the hardness values for Al–Cu–Si (ADC12), $CuAl_2$ (AC2A), and Mg_2Si (AC8A) are low, almost the same as for the α-Al matrix (see their load versus depth). The hardness of the Mg_2Si eutectic structure obtained in Fig. 10c is consistent with the hardness (Mg_2Si) in magnesium alloy reported by Yoo et al. [5]. In their approach, the hardness value (Mg_2Si) is higher than that in the matrix [5]. The reason for the different result may be the different measurement method (micro-Vickers) and different material (Mg alloy). However, further study will be conducted in the future.

Conclusions

Based upon the above experimental approaches using a nano-indentation hardness test, the following conclusions can be drawn:

(1) There is an almost linear relationship between the grain size and hardness although it depends on the casting process, e.g., the hardness for the gravity samples is higher than that for diecast ones. The lower hardness in the diecast samples is caused by cast defects, e.g., porosity.

(2) The material hardness is linearly related to the distance from the grain boundary, the closer to the grain boundary the higher the hardness. The different hardness level is attributed to the different severity of slip resistance of the atoms during the indentation loading.

(3) The material properties in the eutectic structures are different depending on the eutectic system, where the high hardness for the Al–Si-base structure is slightly lower than that for Al–Si–*x*–Fe type eutectic structure, but apparently higher than the hardness for others ($CuAl_2$ and Mg_2Si). The hardness values for $CuAl_2$ and Mg_2Si are almost the same as that in the Al matrix. Such a different hardness of eutectic structure is influenced by different intermetallic compounds.

Acknowledgements The authors would like to acknowledge the technical support of Dr. Jun Kobayashi, Dr. Noriko Muto and Mr. Tatsuya Taki at Akita Prefectural University.

References

1. Mae H, Teng X, Bai Y, Wiezbicki T (2008) Int J Solid Struct 45:1430
2. Polmear IJ (2007) Light alloys from traditional alloys to nanocrystals, 4th edn. Elsevier, London, p 205
3. Okayasu M, Nishi N, Kanazawa K (1998) J Jpn Foundry Eng Soc 70:266 (Japanese)
4. Kim JJ, Kim DH, Shin KS, Kim NJ (1999) Scr Mater 41:333
5. Yoo MS, Kwang SS, Kim NJ (2002) Metall Mater Trans A 35:1629
6. Okayasu M, Takasu S, Yoshie S (2010) J Mater Process Tech 210:1529
7. Chuang TH, Yeh MS, Tsao LC, Tsai TC, Wu CS (2000) Metall Mater Trans A 31:2239
8. Li Z, Samuel AM, Samuel FH, Ravindran C, Valtierra S (2003) J Mater Sci 38:1203. doi:10.1023/A:1022857703995
9. Hertzberg RW (1996) Deformation and fracture mechanics of engineering materials, 4th edn. John Wiley & Sons Inc., New York
10. Osório WR, Goulart PR, Santos GA, Neto CM, Garcia A (2006) Metall Mater Trans A 37:2525
11. Kanazawa K, Okayasu M (1998) Trans Jpn Soc Mech Eng 64:1956 Japanese
12. Iwahori H, Tozawa K, Asano T, Yamamoto Y, Nakamura M, Hashimoto M, Uenishi S (1984) J Jpn Inst Light Met 34:525 Japanese
13. Hekmat-Ardakan A, Ajersch F, Chen X-G (2011) J Mater Sci 46:2370. doi:10.1007/s10853-010-5084-1
14. Shimadzu, Technical Manual for DUH-211 (Shimadzu Co.), p 5-2 (Japanese)
15. Okayasu M, Yoshifuji S, Mizuno M, Hitomi M, Yamazaki H (2009) Int J Cast Metal Res 22:374
16. Okayasu M, Hitomi M, Yamazaki H (2009) J Eur Ceram Soc 29:2369